Agenzia nazionale per le nuove tecnologie, l'energia
e lo sviluppo economico sostenibile

Ministero dello Sviluppo Economico

RICERCA DI SISTEMA ELETTRICO

Caratterizzazione di materiali nucleari tramite analisi dati misure diffusione e diffrazione neutronica

Fabrizio Fiori, Paolo Mariani, Francesco Spinozzi

RdS/2012/163

CARATTERIZZAZIONE DI MATERIALI NUCLEARI TRAMITE ANALISI DATI MISURE DIFFUSIONE E DIFFRAZIONE NEUTRONICA

Fabrizio Fiori, Paolo Mariani, Francesco Spinozzi Università Politecnica delle Marche

Settembre 2012

Report Ricerca di Sistema Elettrico
Accordo di Programma Ministero dello Sviluppo Economico - ENEA
Area: Governo, Gestione e Sviluppo**,** del Sistema Elettrico Nazionale
Progetto: Nuovo Nucleare da Fissione: Collaborazioni Internazionali e sviluppo Competenze in Materia Nucleare
Responsabile del Progetto: Massimo Sepielli,ENEA

PAR 2012
Progetto 1.3.1 - Nuovo Nucleare da Fissione:
collaborazioni internazionali e
competenze in materia nucleare

RELAZIONE FINALE

relativa all'accordo di Collaborazione tra ENEA e
UnivPM - DiSVA
per una attività di ricerca dal titolo:
Caratterizzazione di materiali nucleari tramite analisi dati misure diffusione e diffrazione neutronica

Fabrizio Fiori, Paolo Mariani, Francesco Spinozzi
Università Politecnica delle Marche,
Dipartimento di Scienze della Vita e dell'Ambiente,
via Ranieri 65, 60131 Ancona, Italy

September 26, 2012

Note sulla Relazione Finale

La presente relazione riguarda le attività svolte presso il Dipartimento DiSVA dell'Università Politecnica delle Marche nell'ambito del contratto indicato (scadenza naturale, 30 settembre 2012).

La relazione e' divisa in due parti. Nella prima, viene presentato il lavoro svolto per la la messa a punto di codici di calcolo necessari ad una affidabile interpretazione delle misure SANS condotte su materiali nucleari. I codici sono stati implementati in Fortran in alcune subroutines originali (che sono allegate alla relazione, Appendice A) che sono state inserite nel programma di analisi di dati SAS GENFIT. La solidità e affidabilità del codice sviluppato sono state verificate analizzando spettri SANS di campioni di acciaio prima e dopo irraggiamento, ottenuti sia mediante simulazioni che sperimentalmente, valutando sistematicamente i parametri più significativi e assumendo come unica ipotesi l'esistenza nei materiali di una polidispersione diluita di difetti microstrutturali a fattore di forma sferico. Sia nel caso delle 2 curve simulate che in quello delle 2 curve sperimentali considerate (campioni di Eurofer 97 misurati ad ILL, Grenoble), i risultati ottenuti (in termini di polidispersione e frazione volumica delle diverse famiglie di difetti) sono stati comparati con quelli ottenuti per trasformata indiretta dell'intensità SANS:

$$\frac{d\Sigma}{d\Omega}(q) = (\Delta\rho)^2 \int dR\, N(R)\, [V(R)]^2\, |F(q,R)|^2 \tag{1}$$

dove q è il modulo del momento trasferito, $N(R)$ il numero per unità di volume di centri di dimensioni comprese tra R e $R + dR$, $V(R)$ il loro volume, $|F(q,R)|^2$ il loro fattore di forma (in questo caso assunto sferico) e $(\Delta\rho)^2$ il *contrasto*, ovvero il quadrato della differenza tra la densità di lunghezza di scattering delle inomogeneità e la matrice metallica, calcolata utilizzando il metodo riportato in referenza (1) e più recentemente discusso da Coppola e altri (2–4).

La seconda parte della relazione riguarda l'analisi attraverso il programma FULLPROF di alcune misure di diffrazione neutronica su materiale nucleari di interesse tecnologico. Lo scopo è quello di caratterizzare le fasi cristallografiche presenti nel campione e di quantificarne il contenuto. I risultati ottenuti con FULLPROF hanno permesso di individuare la presenza di nanocristalli di Y_2O_3 (nella forma cubica a corpo centrato, Ia-3) nella matrice di acciaio martensitico Eurofer-97 e di osservare che il loro contributo all'intensità integrata totale del segnale di diffrazione è pienamente compatibile con la composizione nominale del materiale stesso. I dettagli dei risultati discussi e mostrati nella relazione sono contenuti integralmente nella appendice che viene allegata alla presente relazione (Appendice B).

Si precisa infine quanto segue: le considerazioni sul codice MPS si riferiscono all'utilizzo che ne hanno fatto gli autori relativamente agli spettri SANS considerati. Le conclusioni sull'eventuale presenza della fase Y_2O_3 andranno verificate con una accurata analisi del rumore di fondo.

SANS investigations of metallic alloys with different types of inhomogeneities

Introduction

Small-angle neutron scattering (SANS) is a versatile technique for studying structure and size distribution of inhomogeneities of metallic alloys in a wide range of dimensions, from nanometers to micrometers. With respect to X-rays and the corresponding twinned technique (small-angle X-ray scattering, SAXS), the advantage of SANS is the capability of neutrons to deeply penetrate into metallic materials, allowing to get information on their bulk properties. Indeed, neutrons interact with the nucleus of all atoms and the isotropic neutron scattering signal is a complex combination of all the spherical neutron waves originating from any nucleus of the system. However, since SANS is not a local technique but a tool that collects the information of all the components of the system, the structural complexity of metal alloys cannot be completely revealed. From a physical point of view, what can make visible to neutrons the presence of a structural inhomogeneity (*e.g.* precipitates or voids) is the difference between the scattering length density of the j-inhomogeneity, ρ_j, and the one of the bulk materials, ρ_0. This difference is commonly referred to as "the contrast" and written as $\Delta\rho_j$. The simplest cases that can be successfully investigated by means of SANS are systems with a low content of inhomogeneities, namely where their volume fraction, ϕ, is in the order of some percent. In such cases, the contribution due to the interference between neutron waves scattered from distinct particles can be considered negligible and the SANS patterns bring information only on sizes and shapes of the inhomogeneities. Metallic alloys are a typical example of a polydispersed system, where the sizes of the possible inhomogeneities are usually distributed in a wide range of dimensions. In particular, when the morphology of the inhomogeneities is not known or when is not ascertained if the growth of the inhomogeneities follows a specified directionality, the analysis of SANS data cannot be able to get the shape (at low-resolution) of the particles. As a consequence, in terms of geometrical shapes, in studying widely polydispersed systems is not possible to distinguish, for example, among cylinders, cubes, ellipsoids or other simple forms. These kind of systems are generally analyzed in terms of polydispersed spheres and the structural information usually obtained is the distribution function $f(R)$ of the sphere radius R together with the whole volume fraction of the spherical inhomogeneities. To date, the most general approach to describe $f(R)$ is in terms of linear combination of cubic B-splines, which are bell-shaped third degree polynomials defined over a set of equispaced knots either in a linear or in a logarithmic space between the minimum and the maximum values of the sphere radius.

So far, this method has been largely used in the analysis of SANS data, by using numerical codes such as the one developed by Magnani, Puliti and Stefanon (MPS) (1). By this code it is possible to obtain the size distribution of polydispersed spheres in terms of linear combinations of cubic B-spline functions, with the possibility to choose a certain number of input parameters such as the number of splines, the direct-space (R) range, the nuclear contrast, the incoherent background. Anyway this code is based on a "pure two-phase model", that is a distribution of just one type of polydispersed objects inside the matrix, not allowing to take into account the eventual presence of more than one kind of inhomogeneities, with different nuclear contrast with respect to the matrix.

In the present study we have extended the cubic B-splines approach to the investigation of metal alloys which contain up to a maximum of two different kind of inhomogeneities, namely

precipitates and voids, each one characterized by a specific scattering length density. A test case is performed by analyzing the SANS signal of a sample of "Eurofer" alloy before and after being subjected to irradiation in a nuclear reactor. Results are discussed in terms of i) the number of cubic B-splines used and ii) the "regularization" constraint.

Method

The system under investigation is supposed to be composed by a number p of different kinds of diluted and polydispersed inhomogeneities, all with a spherical shape. The nuclear component of the macroscopic differential neutron scattering cross section (SCS) of such a system, provided by a SANS experiment, is expressed by

$$\frac{d\Sigma}{d\Omega}(q) = \sum_{j=1}^{p} n_j P_j(q) + B \tag{2}$$

where $q = 4\pi \sin\theta/\lambda$ is the modulus of the transferred momentum (2θ being the scattering angle and λ the neutron wavelength), n_j is the total number of j-kind particle per unit volume and B is a flat background, due to all the inchoerent scattering processes. $P_j(q)$ is the form factor of the j-kind polydispersed spherical inhomogeneities,

$$P_j(q) = (\Delta\rho_j)^2 \int_{R_{j,\mathrm{mix}}}^{R_{j,\max}} f_j(R) \left[\frac{4}{3}\pi R^3 \Phi(qR)\right]^2 dR \tag{3}$$

$$\Phi(x) = 3\,\frac{\sin x - x\cos x}{x^3} \tag{4}$$

In the Eq. 3, $f_j(R)$ represents the distribution function of the radius of the j-spheres, with the normalisation condition $\int_{R_{j,\min}}^{R_{j,\max}} f_j(R)dR = 1$. In the case of spherical radii possibly distributed over several decades of values (wide polydispersity), it is a common practice to write the function $f_j(R)$ as a linear combination of N cubic B-splines defined in a logarithmic grid,

$$f_j(R) = \frac{N+3}{R_{j,\max} - R_{j,\min}} \sum_{n=1}^{N} c_{j,n} B_{3,n}(\log R) \tag{5}$$

where $B_{3,n}(x)$ is the n-th of N bell-shaped functions defined in a grid of $N+3$ knots equally distributed in the range $\log R_{j,\min} \div \log R_{j,\max}$ (5) (Fig. 1) and $c_{j,n} \geq 0$ (with the normalisation condition $\sum_{n=1}^{N} c_{j,n} = 1$) is the corresponding expansion coefficient of the j-kind of spherical inhomogeneity.

The definition of $B_{3,n}(x)$ ensures that outside the interval $[R_{j,\min}, R_{j,\max}]$ the distribution function $f_j(R)$ is always zero and that it continuously reaches the zero value at $R = R_{j,\min}$ and $R = R_{j,\max}$. Moreover, the flattest condition for the $f_j(R)$ is achieved when all the coefficients $c_{j,n}$ have the same value. The volume fraction of the j-spheres is simply calculated by the integral

$$\phi_j = \frac{4}{3}\pi n_j \int_{R_{j,\min}}^{R_{j,\max}} R^3 f_j(R) dR. \tag{6}$$

However, since volume fractions are obviously limited in the range $[0, 1]$, in a fitting implementation of the method it is much more effective to consider ϕ_j as free parameters and to derive n_j from Eq. 6

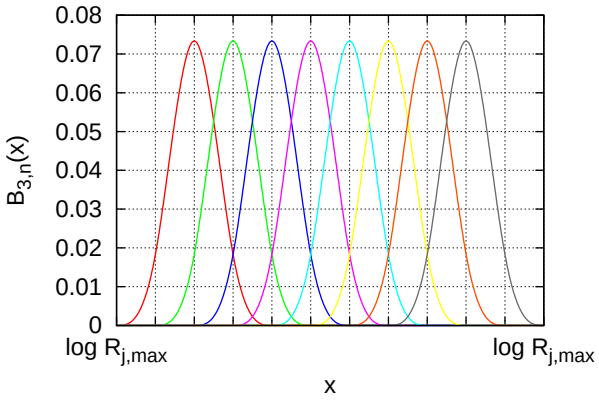

Figure 1: Example of N=8 cubic B-splines functions

In summary, in the case of SANS curves obtained in absolute units (usually cm^{-1}) and when the scattering length densities ρ_j of all the possible inhomogeneities as well as the one of the underlying matrix, ρ_0, are known, the adjustable parameters of the model are the flat background B and, for each j-kind of inhomogeneity, the volume fraction ϕ_j, the radius limits $R_{j,\min}$ and $R_{j,\max}$, and the set of N coefficients $\{c_{j,n}\}$. Optimum values of all these parameters are the ones that minimise the standard reduced χ^2

$$\chi^2 = \frac{1}{N_q - 1} \sum_{k=1}^{N_q} \left\{ \frac{\frac{d\Sigma}{d\Omega}(q_k) - \frac{d\Sigma}{d\Omega}_{\exp}(q_k)}{\sigma_{\exp}(q_k)} \right\}^2 \tag{7}$$

where $\frac{d\Sigma}{d\Omega}_{\exp}(q_k)$ and $\sigma_{\exp}(q_k)$ are the experimental curve and its standard deviation measured for N_q values of the momentum q. As widely discussed by the literature in tackling similar problems (6), there is not a unique solution that minimize χ^2 and, most importantly, many solutions are quite unstable and give rise to large and unphysical oscillations of the distributions $f_j(R)$. One of the very commonly used method to avoid such oscillations is to exploit the so-called "regularization" method (7) based on the calculation of a damping term

$$U = \frac{1}{2} K \sum_{j=1}^{p} \sum_{n=1}^{N-1} (c_{j,n+1} - c_{j,n})^2 \tag{8}$$

which is added to the χ^2 to define a global functional $\mathcal{H}$ to be minimised

$$\mathcal{H} = \chi^2 + U \tag{9}$$

The estimation of the parameter K, which regulates the relative weight of U with respect to χ^2, can be performed in different and sometimes tricky ways. Here we have chosen a very simple cryterion: K is found in such a way that, for statistically acceptable values of $\chi^2 \sim 1$, the value of U is ~ 0.05.

The present method is applied within the software GENFIT (8–11), which is a flexible tool to analyse SAS data with different models or combinations of models. The minimization of $\mathcal{H}$ is carried out in two different steps, the first by using Simulated Annealing method and the second with the Simplex method. Details are given in Ref. (12, 13).

Experimental

SANS experiments have been performed in ILL in Grenoble at the D22 instrument. Two different sample-to-detector distances (2 and 12 m) have been used to cover an extended q-range from 4 10^{-3} to 2.4 10^{-1} Å^{-1} and data have been recored on a 2D 512x512 detector. Samples were placed in a saturating horizontal magnetic field of 1 T (applied perpendicular to the incoming neutron beam) in order to distinguish the nuclear and magnetic SANS cross-sections. According to the set-up, nuclear scattering occurs in the horizontal plane, while nuclear and magnetic scattering occur in the vertical one (the purely magnetic scattering can be then obtained as the difference between the vertical and horizontal SANS cross-sections). After correction for background noise, detector efficiency and attenuation factor, the value of the SANS cross-section in absolute units was obtained by a calibration of the neutron flux, measuring water in a quartz cell, and by means of the ILL standard programs (GRASP software). Two EUROFER 97 samples (a ferritic-martensitic steel, candidate as structural material for the DEMO thermonuclear reactor) have been in particular considered: the first sample was irradiated at 250°C and the damage dose was 16 dpa (displacement-per-atom); the second one was a reference sample, only subjected to thermal processing.

Result and Discussion

Test on simulated SANS data

The method described above has been at first applied to simulated SANS data of a metal alloy. Indeed, two SANS curves have been simulated in a typical q-range detectable at the instrument D22 of ILL (France) by using two configurations (e.g., sample-to-detector distances 2 and 12 m). The simulated curves are shown in Fig. 2 and all the used parameters are reported in the caption: circles represent the SANS curve of an alloy with only one type of inhomogeneity ($p_{sim} = 1$), which are thought to be carbide precipitates with volume fraction $\phi_1 = 0.05$; triangles simulate a SANS curve of a similar alloy (with the same volume fraction of carbide precipitates) subjected to radiation damage, whose effects are supposed to add voids defects ($p_{sim} = 2$) with volume fraction $\phi_2 = 0.01$.

To check the capability of the GENFIT method to get the structural information from the data, the two simulated curves have been analyzed by using diverse parameterization settings, which have been organized in two groups. Within each group, the two SANS curves have been analyzed with three different values of the number of B-splines ($N = 4$, 6 and 8) and two values of the regularization parameters, $K = 0$ and 1. Each fitting is repeated 5 times starting by new SANS curves obtained by a Gaussian sampling of the SCSs within their standard deviations. This procedure allows a robust estimation of the standard deviation of any fitting parameters (14).

Group I: fitting of the simulated SANS curves with the hypothesis of two families of spherical inhomogeneities ($p = 2$, carbide precipitates and voids)

The first group of GENFIT analyses have been carried out by using the hypothesis that two kinds of spherical inhomogeneities ($p = 2$, i.e. precipitates, $j = 1$, and voids, $j = 2$) exist in the alloy. Corresponding scattering length densities ρ_j, together with the matrix one, ρ_0, have

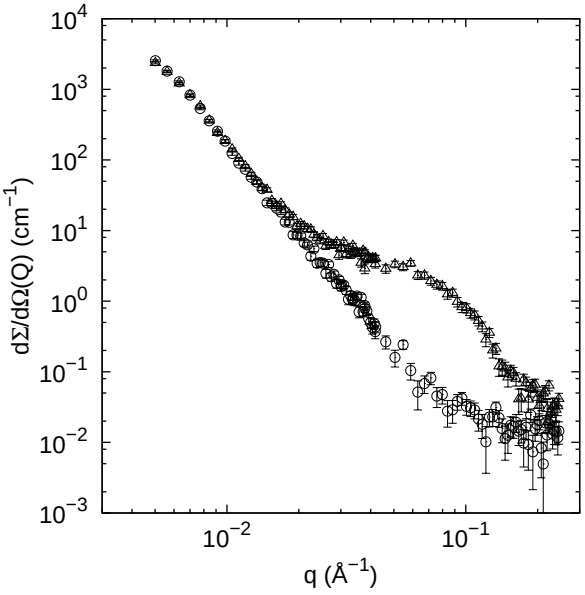

Figure 2: Simulated SANS curves calculated with Eq. 2. Standard deviation are calculated by the expression $\sigma_{\rm exp}(q_k) = 0.03 \left[\frac{d\Sigma}{d\Omega}_{\rm exp}(q_1)\right]^{0.2} \left[\frac{d\Sigma}{d\Omega}_{\rm exp}(q_k)\right]^{0.8}$ and simulated values are randomly moved through a Montecarlo Gaussian sampling. Circles: reference alloy, $\rho_1 = 5.30 \cdot 10^{-6}$ Å^{-2}, $\rho_0 = 7.55 \cdot 10^{-6}$ Å^{-2}, $\phi_1 = 0.05$, $B = 0.015$ cm^{-1}, $R_{1,\rm min} = 10$ Å, $R_{1,\rm max} = 800$ Å, $N = 8$, $c_{1,1} = 0.153$, $c_{1,2} = 0.136$, $c_{1,3} = 0.119$, $c_{1,4} = 0.102$, $c_{1,5} = 0.119$, $c_{1,6} = 0.136$, $c_{1,7} = 0.153$, $c_{1,8} = 0.085$. Triangles: irradiated alloy, $\rho_1 = 5.30 \cdot 10^{-6}$ Å^{-2}, $\rho_2 = 0$, $\rho_0 = 7.55 \cdot 10^{-6}$ Å^{-2}, $\phi_1 = 0.05$, $\phi_2 = 0.01$, $B = 0.015$ cm^{-1}, $R_{1,\rm min} = 10$ Å, $R_{1,\rm max} = 800$ Å, $R_{2,\rm min} = 5$ Å, $R_{2,\rm max} = 40$ Å, $N = 8$, $c_{1,1} = 0.153$, $c_{1,2} = 0.136$, $c_{1,3} = 0.119$, $c_{1,4} = 0.102$, $c_{1,5} = 0.119$, $c_{1,6} = 0.136$, $c_{1,7} = 0.153$, $c_{1,8} = 0.085$, $c_{2,1} = 0.189$, $c_{2,2} = 0.162$, $c_{2,3} = 0.135$, $c_{2,4} = 0.108$, $c_{2,5} = 0.081$, $c_{2,6} = 0.081$, $c_{2,7} = 0.108$, $c_{2,8} = 0.135$.

		a	b	c	d	e	f
χ^2		1.02	1.04	1.04	1.04	1.03	1.04
U		0	0.44	0	0.02	0	0.02
$\mathcal{H}$		1.02	1.37	1.04	1.08	1.03	1.05
B		0.0141±0.0008	0.014±0.001	0.0141±0.0006	0.0141±0.0006	0.014±0.002	0.0141±0.0009
ϕ_1		0.051±0.002	0.050±0.001	0.051±0.001	0.051±0.001	0.052±0.001	0.051±0.002
$R_{1,\mathrm{mix}}$	(Å)	30±20	96±5	40±30	20±10	31±9	10±6
$R_{1,\mathrm{max}}$	(Å)	820±60	760±80	800±100	810±30	880±60	800±80
$c_{1,1}$		0.0±0.1	0.33±0.06	0.00±0.07	0.19±0.04	0.12±0.04	0.15±0.03
$c_{1,2}$		0	0.31±0.06	0.19±0.08	0.20±0.04	0.16±0.03	0.16±0.03
$c_{1,3}$		0.6±0.2	0.24±0.05	0.17±0.06	0.10±0.05	0.00±0.09	0.17±0.03
$c_{1,4}$		0.4±0.2	0.12±0.03	0.28±0.08	0.12±0.04	0.11±0.05	0.11±0.03
$c_{1,5}$		0	0	0.25±0.07	0.23±0.07	0.20±0.06	0.06±0.04
$c_{1,6}$		0	0	0.09±0.03	0.16±0.05	0.22±0.07	0.10±0.05
$c_{1,7}$		0	0	0	0	0.15±0.03	0.16±0.03
$c_{1,8}$		0	0	0	0	0.03±0.03	0.09±0.03
ϕ_2		$(2\pm2)\cdot10^{-5}$	$(19\pm7)\cdot10^{-6}$	$(1\pm1)\cdot10^{-5}$	$(2\pm6)\cdot10^{-6}$	$(1\pm4)\cdot10^{-5}$	$(0\pm3)\cdot10^{-5}$
$R_{2,\mathrm{mix}}$	(Å)	10±1	8±2	10±3	10±1	2±3	7±3
$R_{2,\mathrm{max}}$	(Å)	100±20	100±1	91±5	30±30	30±20	60±20
$c_{2,1}$		0.4±0.1	0.33±0.08	0.18±0.06	0.25±0.03	0.15±0.06	0.15±0.02
$c_{2,2}$		0.2±0.1	0.30±0.08	0.15±0.07	0.19±0.02	0.08±0.06	0.14±0.02
$c_{2,3}$		0	0.23±0.07	0.15±0.04	0.19±0.03	0.15±0.04	0.11±0.02
$c_{2,4}$		0.4±0.1	0.13±0.05	0.17±0.08	0.13±0.05	0.09±0.03	0.09±0.03
$c_{2,5}$		0	0	0.13±0.06	0.12±0.03	0.16±0.04	0.12±0.02
$c_{2,6}$		0	0	0.21±0.05	0.13±0.02	0.14±0.05	0.13±0.01
$c_{2,7}$		0	0	0	0	0.10±0.04	0.13±0.01
$c_{2,8}$		0	0	0	0	0.13±0.04	0.13±0.01

Table 1: Fitting parameters from the analysis with $p = 2$ of the simulated SANS curve for the reference alloy ($p_{sim} = 1$), group I. a) $N = 4$, $K = 0$; b) $N = 4$, $K = 1$; c) $N = 6$, $K = 0$; d) $N = 6$, $K = 1$; e) $N = 8$, $K = 0$; f) $N = 8$, $K = 1$.

been fixed to the values calculated for carbide precipitates, voids and metal alloy, as used in simulations (see the caption of Fig. 2). All resulting parameters are reported in Tables 1-2.

Fitting curves and volume distributions functions are shown in Figs. 3-5 and in Figs. 4-6, respectively.

All the six analyses (a-f) of the simulated curve with $p_{sim} = 1$ give very good results, as revealed by the values of χ^2 close to 1 (Tab. 1). Noticeable is the fact that the volume fractions of the precipitates, ϕ_1, are in all cases practically equal to the value used in the simulation, 0.05, with relative errors of $\sim 2\%$. Within the experimental errors, also the upper and lower limits of the radius of precipitates R turn out to be close to the values used for the input, 10 and 800 Å, respectively. On the other hand, the volume fractions of the voids, ϕ_2, which do not exist in the simulated curve, are all in the order of $10^{-5} - 10^{-6}$, with very high relative errors, clearly indicating that the fitting do not need the second form factor to reproduce the data. This result can be also checked by looking to Fig. 4, where the volume distribution functions of voids $\frac{4}{3}\pi n_2 f_2(R)R^3$ (red dotted lines) are almost 0 in all the range of the radius R. In the same figure it can be appreciated the similarity between the simulated volume distribution functions of precipitates $\frac{4}{3}\pi n_1 f_1(R)R^3$ (black curve) and the one given by the analysis (solid red curve). In particular, also by using $N = 4$ B-splines (cases a and b) the result is good. The effect of the regularization can be observed by comparing the case b with the case a (for $N = 4$) as well as the case d with c ($N = 6$) and finally f with e ($N = 8$): in the presence of the regularization constraint the uncertainties on the $\frac{4}{3}\pi n_1 f_1(R)R^3$ profile decreases.

The six analyses of this group have been then applied to the simulated curve for the irradiated alloy sample, e.g. in the presence of both precipitates and voids ($p_{sim} = 2$), shown in Fig. 2 (triangles). Fitted curves (Fig. 5, cases a-f) are very good, as quantitatively confirmed by the values of χ^2 reported in Table 2. In all cases, the volume fractions ϕ_1 and ϕ_2 of pre-

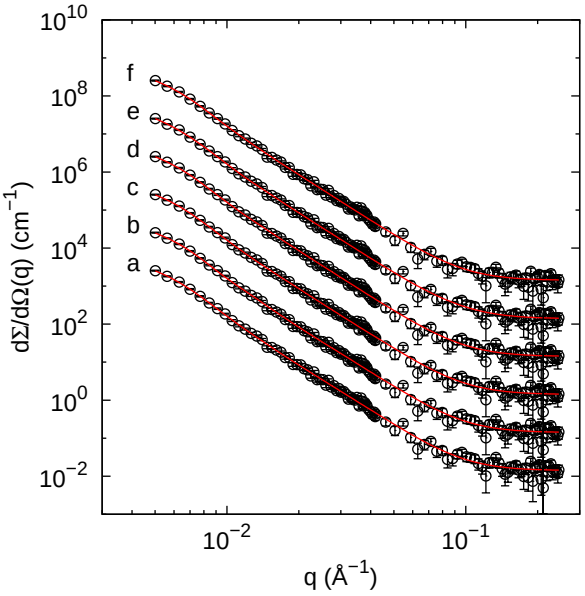

Figure 3: Fitting curves of the simulated SANS curve for the reference alloy ($p_{sim} = 1$) obtained by using $p = 2$, group I. Curves are scaled by a factor 10 for clarity. See the caption of Table 1 for the meaning of cases a-f.

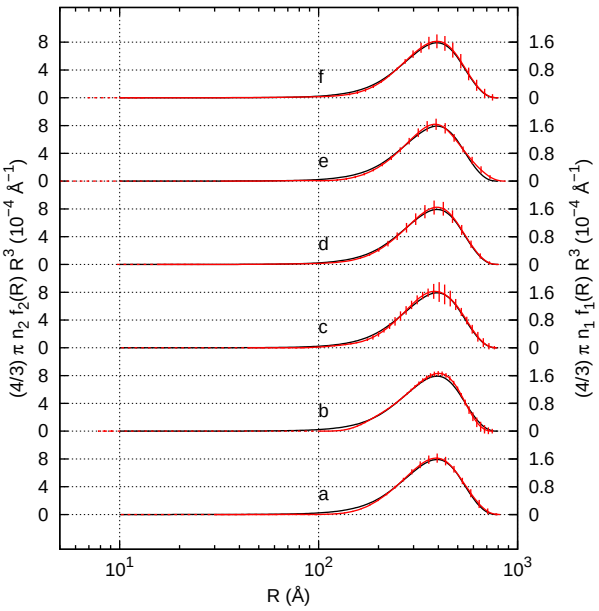

Figure 4: Volume distribution functions obtained by the analysis with $p = 2$ of the simulated SANS curve for the reference alloy ($p_{sim} = 1$), group I. Black and red solid lines refer to the simulated and analyzed distributions of precipitates ($j = 1$), respectively. Red dotted lines refer to the analyzed distributions of voids ($j = 2$). See the caption of Table 1 for the meaning of cases a-f.

		a	b	c	d	e	f
χ^2		0.99	1.07	0.99	1.00	0.99	0.98
U		0	0.38	0	0.04	0	0.01
$\mathcal{H}$		0.99	1.43	0.99	1.04	0.99	0.99
B		0.019±0.003	0.019±0.003	0.017±0.003	0.019±0.003	0.022±0.003	0.020±0.003
ϕ_1		0.0493±0.0005	0.049±0.001	0.0488±0.0005	0.050±0.001	0.0496±0.0004	0.0490±0.0006
$R_{1,\mathrm{mix}}$	(Å)	17±7	40±10	12±6	10±10	1±1	9±4
$R_{1,\mathrm{max}}$	(Å)	810±20	780±30	780±30	820±60	830±20	780±30
$c_{1,1}$		0.4±0.1	0.30±0.03	0.18±0.04	0.22±0.07	0.10±0.06	0.09±0.03
$c_{1,2}$		0.07±0.09	0.28±0.03	0.11±0.06	0.19±0.08	0.14±0.07	0.15±0.03
$c_{1,3}$		0.2±0.1	0.25±0.04	0.09±0.09	0.13±0.09	0.20±0.07	0.14±0.02
$c_{1,4}$		0.3±0.1	0.17±0.04	0.21±0.04	0.1±0.1	0.21±0.07	0.12±0.03
$c_{1,5}$		0	0	0.21±0.05	0.13±0.09	0.02±0.09	0.14±0.03
$c_{1,6}$		0	0	0.19±0.04	0.21±0.09	0.04±0.06	0.10±0.03
$c_{1,7}$		0	0	0	0	0.09±0.07	0.16±0.04
$c_{1,8}$		0	0	0	0	0.21±0.05	0.09±0.03
ϕ_2		0.0098±0.0003	0.0096±0.0001	0.0100±0.0003	0.0098±0.0003	0.0096±0.0007	0.0098±0.0003
$R_{2,\mathrm{mix}}$	(Å)	6±1	10±2	5±3	9±2	8±2	8±2
$R_{2,\mathrm{max}}$	(Å)	42±1	43±2	41±2	40±3	59±8	38.5±0.9
$c_{2,1}$		0.29±0.08	0.29±0.07	0.25±0.06	0.18±0.04	0	0.13±0.03
$c_{2,2}$		0.3±0.1	0.28±0.07	0.20±0.06	0.16±0.03	0	0.12±0.02
$c_{2,3}$		0.0±0.2	0.25±0.07	0.23±0.08	0.16±0.03	0.2±0.1	0.07±0.03
$c_{2,4}$		0.4±0.1	0.17±0.06	0.06±0.09	0.18±0.03	0.3±0.1	0.10±0.03
$c_{2,5}$		0	0	0.0±0.1	0.18±0.03	0.3±0.1	0.13±0.02
$c_{2,6}$		0	0	0.21±0.05	0.15±0.04	0.3±0.1	0.15±0.03
$c_{2,7}$		0	0	0	0	0	0.16±0.02
$c_{2,8}$		0	0	0	0	0	0.14±0.03

Table 2: Fitting parameters from the analysis with $p = 2$ of the simulated SANS curve for the irradiated alloy ($p_{sim} = 2$), group I. See the caption of Table 1 for the meaning of cases a-f.

cipitates and voids have turned out to be very close to the values used in the simulation, 0.05 and 0.01, respectively, with relative errors always lower than 2%, indicating a good capability of the fitting method to extract this kind of information out of the SANS curve. Moreover, for all the six cases, lower and upper values of the inhomogeneities' radius ($R_{j,\mathrm{min}}$ and $R_{j,\mathrm{max}}$) are found by GENFIT to be very close to the values used in the simulated curve (10 and 800 Å for $j = 1$; 5 and 40 Å for $j = 2$). A more detailed analysis of the results can be performed by looking to the trends of the volume distribution functions of the inhomogeneities, shown in Fig. 6. Notice that, for a better visualization of the results, two different scales in the y-axis have been selected: on the right the volume distribution functions of the precipitates are reported (solid lines), whereas on the left the ones of the voids (dotted lines) are shown. The case f, related to a number $N = 8$ of cubic B-splines with the regularization constraint ($K = 1$), shows the best overlap between the black and the red functions, corresponding to simulated and analyzed results. By switching off the regularization (case e) a slightly increase of the uncertainty occurs. Cases c and d ($N = 6$, with and without regularization) make it even more clear the improvement carried by the regularization algorithm. A similar effect can also be appreciated with $N = 4$ (cases a and b). However, noticeable is the fact that by using only $N = 4$, peak positions and overall shape of the volume distribution functions $\frac{4}{3}\pi n_j f_j(R)R^3$ are nicely assessed by GENFIT.

Group II: fitting of the simulated SANS curves with the hypothesis of one family of spherical inhomogeneities ($p = 1$) of unknown origin

In the second group, the GENFIT fitting analysis of the two simulated SANS curves (shown in Fig. 2) has been performed considering the presence of only one kind of inhomogeneity ($p = 1$), with a unique effective scattering length density ρ_1, which is considered to be between the two

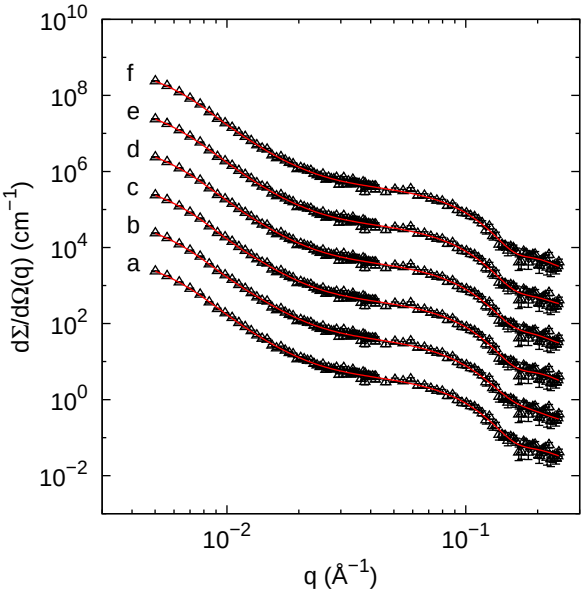

Figure 5: Fitting curves of the simulated SANS curve for the irradiated alloy ($p_{sim} = 2$) obtained by using $p = 2$, group I. Curves are scaled by a factor 10 for clarity. See the caption of Table 1 for the meaning of cases a-f.

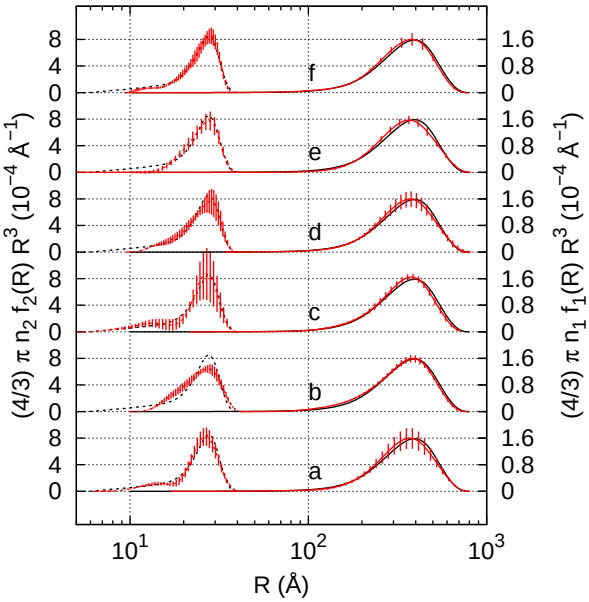

Figure 6: Volume distribution functions obtained by the analysis with $p = 2$ of the simulated SANS curve for the irradiated sample ($p_{sim} = 2$), group I. Black and red solid lines refer to the simulated and analyzed distributions of precipitates ($j = 1$), respectively. Black and red dotted lines refer to the simulated and analyzed distributions of voids ($j = 2$), respectively. See the caption of Table 1 for the meaning of cases a-f.

		a	b	c	d	e	f
χ^2		1.03	1.04	1.03	1.03	1.03	1.04
U		0	0.02	0	0.01	0	0.02
$\mathcal{H}$		1.03	1.06	1.03	1.04	1.03	1.05
B		0.0142±0.0007	0.0142±0.0005	0.014±0.001	0.0142±0.0008	0.0142±0.0003	0.0141±0.0005
ρ_1	(10^{-6} Å^{-2})	5.0±0.2	4.9±0.7	2.7±0.7	5.3±0.6	4.9±0.3	5.2±0.4
ϕ_1		0.041±0.007	0.04±0.01	0.011±0.005	0.05±0.01	0.039±0.006	0.05±0.01
$R_{1,\mathrm{mix}}$	(Å)	30±30	98±4	80±30	100±4	100±30	30±30
$R_{1,\mathrm{max}}$	(Å)	820±40	810±40	920±60	880±60	1000±80	980±90
$c_{1,1}$		0.34±0.09	0.4±0.1	0	0.24±0.04	0.17±0.09	0.17±0.07
$c_{1,2}$		0	0.3±0.1	0.3±0.2	0.25±0.05	0.18±0.08	0.14±0.05
$c_{1,3}$		0.4±0.1	0.25±0.08	0.3±0.1	0.24±0.03	0.21±0.06	0.10±0.05
$c_{1,4}$		0.3±0.1	0.08±0.03	0.3±0.1	0.18±0.05	0.20±0.08	0.08±0.06
$c_{1,5}$		0	0	0.1±0.1	0.09±0.03	0.14±0.05	0.17±0.08
$c_{1,6}$		0	0	0.02±0.08	0.014±0.006	0.08±0.06	0.20±0.07
$c_{1,7}$		0	0	0	0	0.01±0.05	0.13±0.05
$c_{1,8}$		0	0	0	0	0.003±0.008	0.013±0.007

Table 3: Fitting parameters from the analysis with $p = 1$ of the simulated SANS curve for the reference alloy ($p_{sim} = 1$), group II. a) $N = 4$, $K = 0$; b) $N = 4$, $K = 1$; c) $N = 6$, $K = 0$; d) $N = 6$, $K = 1$; e) $N = 8$, $K = 0$; f) $N = 8$, $K = 1$.

values which corresponds to carbide precipitates and voids ($\rho_1 = 5.30 \cdot 10^{-6}$ Å^{-2} and $\rho_1 = 0$, respectively), and with ρ_0 fixed to the value for the metal alloy ($7.55 \cdot 10^{-6}$ Å^{-2}), as used in the simulation.

Fitting parameters obtained by the six GENFIT analyses are reported in Tables 3-4. Fitting curves and distributions functions are shown in Figs. 7-9 and in Figs. 8-10, respectively.

As expected, fitting curves of the SANS profile simulated for the reference sample, e.g. a sample with only one kind of inhomogeneity (precipitates, $p_{sim} = 1$), for all the six kinds of parameterization (a-f) are good and acceptables, as clearly shown in Fig. 7. Looking to the fitting parameters (Table 3), it can be derived that only in the case d and f, both with the regularization option and with $N = 6$ and $N = 8$, respectively, the value of ϕ_1 obtained by the GENFIT analysis has turned out to be close to the value 0.05 used in the simulation. In such cases, also the scattering length densities, ρ_1, extracted by the analysis is close to the value used in the input SANS curve, ($\rho_1 = 5.30 \cdot 10^{-6}$ Å^{-2}, see the caption of Fig. 2). This results is confirmed by looking to the agreement of simulated and analyzed volume distribution functions, as reported in Fig. 8, cases d and f. A straightforward indication is that, in the case of just one type of inhomogeneity and whether the value of its scattering length density ρ_1 is known or fixed, it is possible to derive reliable values of the volume fraction ϕ_1 of such inhomogeneity in the sample.

We turn now to discuss the result of the GENFIT analyses of the SANS curve for the irradiated alloy sample, simulated by considering the presence of two kind of inhomogeneities, precipitates and voids, each one with a proper scattering length density (see Fig. 2, triangles). The fitting analysis is however based on the hypothesis that only one type of inhomogeneity exists in the sample. At a first look, fitted curves, reported in Fig. 9, seem acceptable, however, by carefully observing the results, it is evident that there are ranges of q where the fitting curves are systematically under or over the simulated points. This behavior is much more evident by looking to the residual plots, reported in Fig. 11, lower frame, compared with the residual plots of the GENFIT analyses of group I (Fig. 11, upper frame). A further evidence of not completely satisfactory results is the value of the χ^2s (Table 4) in all cases greater than the value obtained the analyses of group I (Table 2).

In Fig. 10 the unique volume distribution function (solid red curve) is compared with the ones of used in the simulated SANS curve (solid black curve for precipitates and dotted black

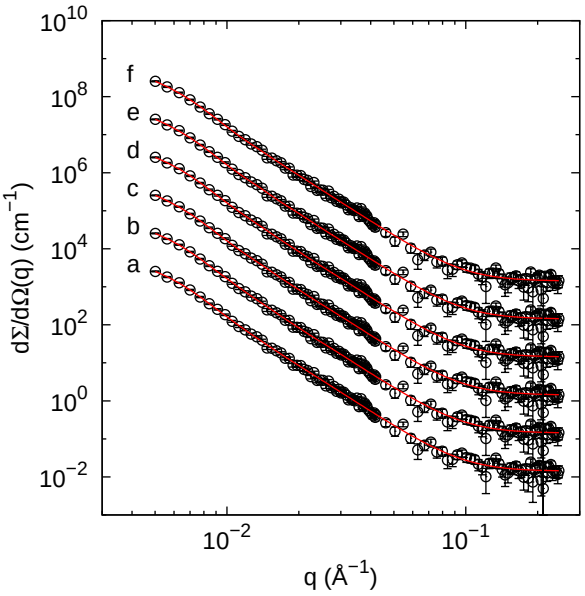

Figure 7: Fitting curves of the simulated SANS curve for the reference alloy ($p_{sim} = 1$) obtained by using $p = 1$, group II. Curves are scaled by a factor 10 for clarity. See the caption of Table 3 for the meaning of cases a-f.

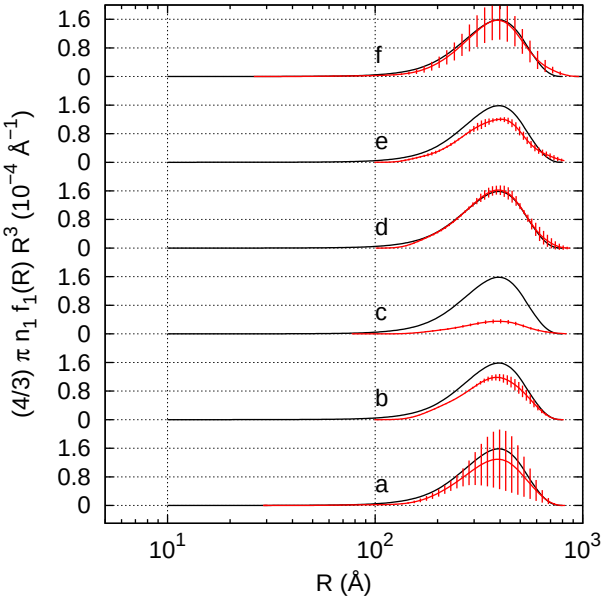

Figure 8: Volume distribution functions obtained by the analysis with $p = 1$ of the simulated SANS curve for the reference alloy ($p_{sim} = 1$), group II. Black and red solid lines refer to the simulated and analyzed distributions of inhomogeneity, respectively.

		a	b	c	d	e	f
χ^2		2.05	2.30	1.45	1.51	1.53	1.36
U		0	0.50	0	0.10	0	0.06
$\mathcal{H}$		2.05	2.80	1.45	1.61	1.53	1.46
B		0.010±0.003	0.100±0.005	0.015±0.003	0.012±0.006	0.0161±0.0009	0.015±0.002
ρ_1	(10^{-6} Å^{-2})	1.8±0.2	5.27±0.09	5.0±0.3	4.2±0.1	3.5±0.7	2.4±0.5
ϕ_1		0.024±0.001	0.17±0.01	0.12±0.02	0.072±0.005	0.047±0.009	0.030±0.009
$R_{1,\mathrm{mix}}$	(Å)	1.26±0.02	1.06±0.09	1.77±0.05	1.8±0.3	1.9±0.2	1.9±0.3
$R_{1,\mathrm{max}}$	(Å)	1000.00±0.03	999.95±0.02	862±8	860±40	770±40	800±20
$c_{1,1}$		$(999995\pm3)\cdot10^{-6}$	$(99997\pm1)\cdot10^{-5}$	0.1±0.3	0.56±0.06	0.31±0.05	0.33±0.04
$c_{1,2}$		0	0	0.9±0.3	0.44±0.06	0.21±0.07	0.26±0.06
$c_{1,3}$		0	0	0	0	0.48±0.05	0.41±0.04
$c_{1,4}$		0	0	0	0	0.002±0.001	0.00±0.01
$c_{1,5}$		0	0	0	0	0	0
$c_{1,6}$		0	0	0	0	0	0
$c_{1,7}$		0	0	0	0	0	0
$c_{1,8}$		0	0	0	0	0	0

Table 4: Fitting parameters from the analysis with $p = 1$ of the simulated SANS curve for the irradiated alloy ($p_{sim} = 2$), group II. See the caption of Table 3 for the meaning of cases a-f.

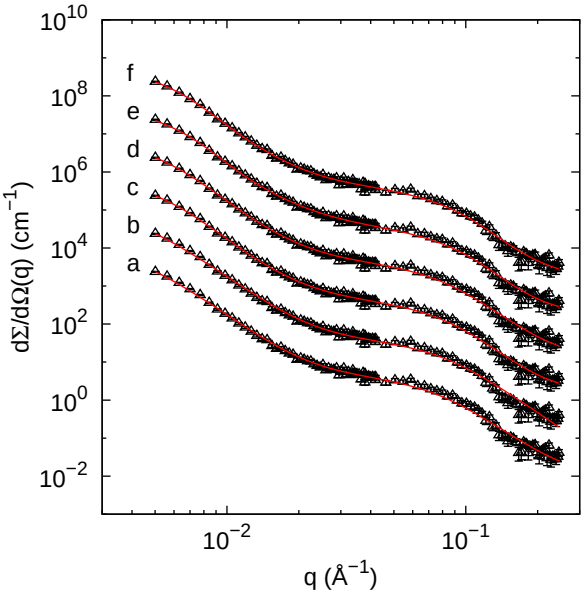

Figure 9: Fitting curves of the simulated SANS curve for the irradiated alloy ($p_{sim} = 2$) obtained by using $p = 1$, group II. Curves are scaled by a factor 10 for clarity. See the caption of Table 3 for the meaning of cases a-f.

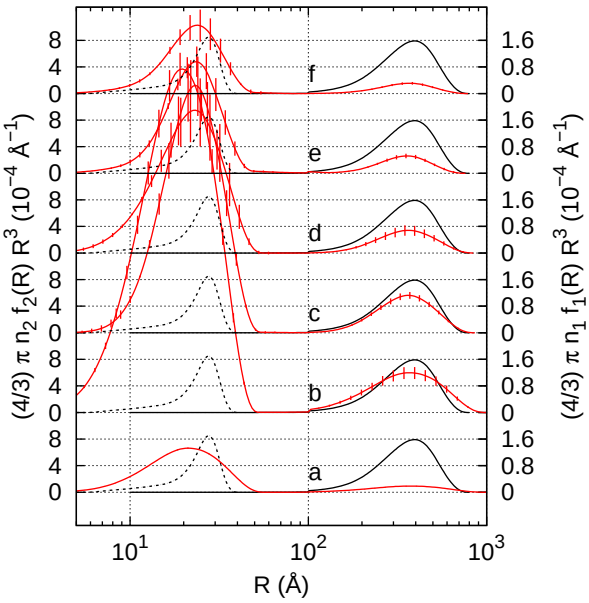

Figure 10: Volume distribution functions obtained by the analysis with $p = 1$ of the simulated SANS curve for the irradiated sample ($p_{sim} = 2$), group II. Black and red solid lines refer to the simulated and analyzed distributions of inhomogeneities, respectively. Black dotted line refers to the simulated distributions of voids ($j = 2$). See the caption of Table 3 for the meaning of cases a-f.

curve for voids): it is evident that only peaks' positions are, on average, recovered but not their heights. In particular, the peak at the lowest values of R, corresponding to voids, is much higher than the simulated peak. This fact can be easily explained: since, in the R range where voids exist, the contrast used in the analysis is lower than the one used in the simulation, the populations of the unique inhomogeneity is increased by GENFIT in order to obtain a good fit to the SANS curve. For the same reason, the height of the red peak at the largest R decreases. It is also clear that in such conditions, the volume fractions ϕ_1 obtained by the analyses (see Table 4) are not comparable with the one of precipitates and voids adopted in the simulation.

Results from the fitting test on the simulated SANS curves

The main result of the simulation tests is that by analyzing a SANS curve of a polydispersed system with more than one type of inhomogeneity with the hypothesis that all the particles can be described by only one average contrast, the information that is derived on particle size distribution is only qualitative and the obtained volume fraction is widely underestimated or overestimated.

Test on experimental SANS data

The same GENFIT analyses, based on cases a-f (see the caption of Table 1) and executed over simulated SANS data for reference and irradiated alloys, have been applied over two experimental SANS curves, corresponding to two EUROFER 97 samples (a ferritic-martensitic steel, candidate as structural material for the DEMO thermonuclear reactor). The first curve

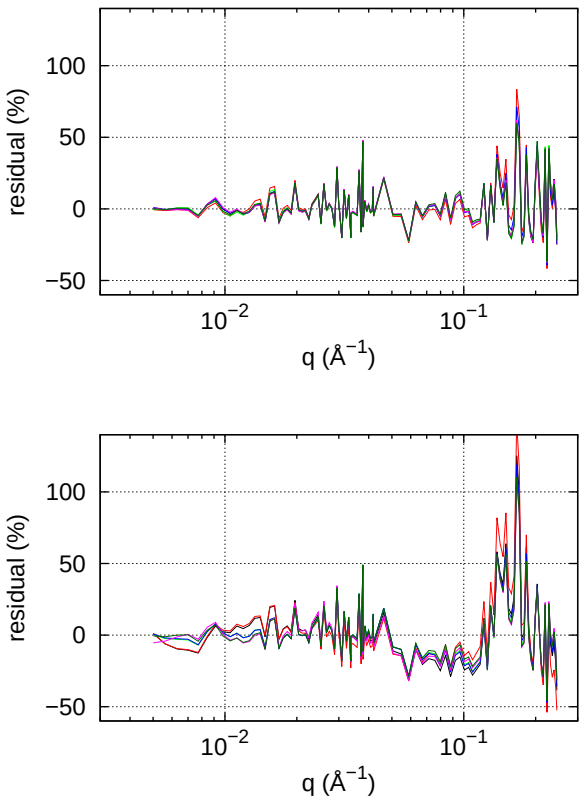

Figure 11: Residual plots, $[\frac{d\Sigma}{d\Omega}(q) - \frac{d\Sigma}{d\Omega}_{\rm exp}(q)]/\frac{d\Sigma}{d\Omega}_{\rm exp}(q)$, of the GENFIT analyes shown in Fig. 5 (upper frame) and in Fig. 9 (lower frame). Black curves, case a. Red curves, case b. Green curves, case c. Blue curves, case d. Magenta curves, case e. Dark-green curves, case f.

has been obtained by a reference sample, only subjected to thermal processing at 250°C, the second curve corresponds to a EUROFER 97 sample subjected to the same thermal processing but irradiated with a damage dose of 16 dpa (displacement-per-atom).

As a comparison, the two SANS curves have been also analyzed by us with the MPS software, by using $N = 4$, 6 and 8 cubic B-splines, defined in a logarhitmic scale between two fixed bounds of the sphere radius, 1 and 2000 Å, respectively. In order to perform a proper comparison between the volume distribution functions obtained with GENFIT and with MPS, the contrast $(\Delta\rho)^2$, used in the MPS software as input parameter, has been fixed to the average value found by GENFIT. In particular, for the group I analyses of GENFIT, the average scattering length density of precipitates and voids is $[(\rho_1\phi_1 + \rho_2\phi_2)/(\phi_1 + \phi_2) - \rho_0]^2$, where the values of ρ_j are the ones adopted in the simulated curves (see the caption of Fig. 2) and ϕ_j are fitting results of GENFIT. On the other hand, for the group II analyses, the constrast is simply $(\rho_1 - \rho_0)^2$, being ρ_1 the fitted value of the unique kind of inhomogeneity obtained by GENFIT. A systematic comparison between the results of the two method has been performed, as described in the following sections.

Group I: fitting of the experimental SANS curves with the hypothesis of two families of spherical inhomogeneities ($p = 2$, carbide precipitates and voids)

The first group of GENFIT analyses have been carried out by using the hypothesis that two kinds of spherical inhomogeneities (i.e. precipitates, $j = 1$, and voids, $j = 2$) exist in the two samples. Corresponding scattering length densities ρ_j, together with the matrix one, ρ_0, have been fixed to the nominal values for carbide precipitates, voids and metal alloy, as used in the previous analysis (see the caption of Fig. 2).

All resulting parameters are reported in Tables 5-6. Fitting curves and volume distributions functions are shown in Figs. 12-14 and in Figs. 13-15, respectively, and compared with the results obtained by us with the MPS software.

At first, we consider the results obtained by analyzing the reference sample. The GENFIT fitted curves, reported as solid red curves in Fig. 12, are all quite good, as also shown by the corresponding values of χ^2 (see Table 5). The volume fraction ϕ_1 of precipitates has been found almost independent on the number of splines and on the regularization option, with an average value of 0.0317 ± 0.0006. On the contrary, the volume fraction ϕ_2 of the voids is almost zero in all cases, as expected. thermal treatment only induces the presence of carbide precipitates. Fitting results obtained by us with MPS are the blue curves reported in Fig. 12: only with $N = 8$ splines the agreement is acceptable (cases e and f).

We look now to to the volume distribution functions, reported in Fig. 13. First, it is very clear that the dotted red lines, representing the voids, are close to zero for all cases. Second, the solid red curves, referring to the precipitates, show a defined peak, whose position and intensity do not change with N and that becomes less modulated and less uncertain in the case of regularization. Third, for the cases e and f, the blu lines obtained with MPS are very close to the red ones, indicating that both methods not only are able to find out a good fit to the data but give also similar distributions of the unique type of inhomogeneity present in the sample. Interestingly, the volume fraction calculated by MPS (see Table 5) for $N = 8$ is found to be 0.028 , very close to the one obtained by GENFIT (0.0317 ± 0.0006).

All the analyses performed by us with both GENFIT and MPS on the not-irradiated, reference sample have been then applied to the SANS curve for the irradiated sample. Fitting curves obtained with GENFIT are reported as solid red lines in Fig. 14: in all cases the agreement with

		a	b	c	d	e	f
χ^2		1.20	1.14	1.16	1.11	1.13	1.18
U		0	0.36	0	0.06	0	0.02
$\mathcal{H}$		1.20	1.48	1.16	1.16	1.13	1.21
B		0.0087±0.0009	0.0101±0.0003	0.0101±0.0003	0.0100±0.0002	0.0101±0.0005	0.0100±0.0005
ϕ_1		0.032±0.001	0.0314±0.0008	0.032±0.002	0.0316±0.0008	0.031±0.001	0.032±0.001
$R_{1,\mathrm{mix}}$	(Å)	20±10	100±30	10±20	60±20	100±20	20±10
$R_{1,\mathrm{max}}$	(Å)	1330±60	1220±30	1330±70	1210±70	1420±80	2000±200
$c_{1,1}$		0.0±0.3	0.33±0.05	0.3±0.1	0.04±0.05	0.20±0.06	0.24±0.05
$c_{1,2}$		0	0.32±0.04	0.3±0.1	0.08±0.06	0.04±0.02	0.13±0.04
$c_{1,3}$		0.5±0.2	0.24±0.03	0	0.24±0.08	0.2±0.1	0.08±0.07
$c_{1,4}$		0.5±0.2	0.11±0.02	0	0.34±0.07	0.22±0.08	0.07±0.06
$c_{1,5}$		0	0	0.30±0.08	0.19±0.05	0.18±0.04	0.20±0.06
$c_{1,6}$		0	0	0.16±0.06	0.10±0.03	0.08±0.03	0.18±0.04
$c_{1,7}$		0	0	0	0	0.05±0.01	0.09±0.02
$c_{1,8}$		0	0	0	0	0	0
ϕ_2		0.0001±0.0003	$(0\pm3)\cdot10^{-6}$	$(0\pm5)\cdot10^{-6}$	$(4\pm2)\cdot10^{-6}$	$(1\pm2)\cdot10^{-6}$	$(0\pm1)\cdot10^{-5}$
$R_{2,\mathrm{mix}}$	(Å)	1±2	10±3	9±4	1±4	3±4	2±4
$R_{2,\mathrm{max}}$	(Å)	20±20	100±20	100±20	60±20	100±10	50±10
$c_{2,1}$		0.2±0.1	0.34±0.04	0.15±0.05	0.19±0.02	0.20±0.08	0.12±0.03
$c_{2,2}$		0.12±0.09	0.30±0.04	0.19±0.05	0.17±0.02	0.14±0.04	0.07±0.03
$c_{2,3}$		0.29±0.07	0.23±0.03	0.15±0.06	0.19±0.03	0.10±0.07	0.12±0.01
$c_{2,4}$		0.42±0.09	0.13±0.02	0.11±0.07	0.18±0.03	0.18±0.04	0.09±0.04
$c_{2,5}$		0	0	0.20±0.07	0.19±0.03	0.13±0.06	0.11±0.03
$c_{2,6}$		0	0	0.20±0.07	0.09±0.01	0.00±0.07	0.16±0.03
$c_{2,7}$		0	0	0	0	0.11±0.05	0.17±0.03
$c_{2,8}$		0	0	0	0	0.13±0.05	0.16±0.03
ϕ_{MPS}		0.009	0.009	0.018	0.018	0.028	0.028

Table 5: Fitting parameters from the GENFIT analyses with $p = 2$ of the experimental SANS curve for the not-irradiated, reference sample, group I. ϕ_{MPS}s refer to the MPS analyses. a) $N = 4$, $K = 0$; b) $N = 4$, $K = 1$; c) $N = 6$, $K = 0$; d) $N = 6$, $K = 1$; e) $N = 8$, $K = 0$; f) $N = 8$, $K = 1$.

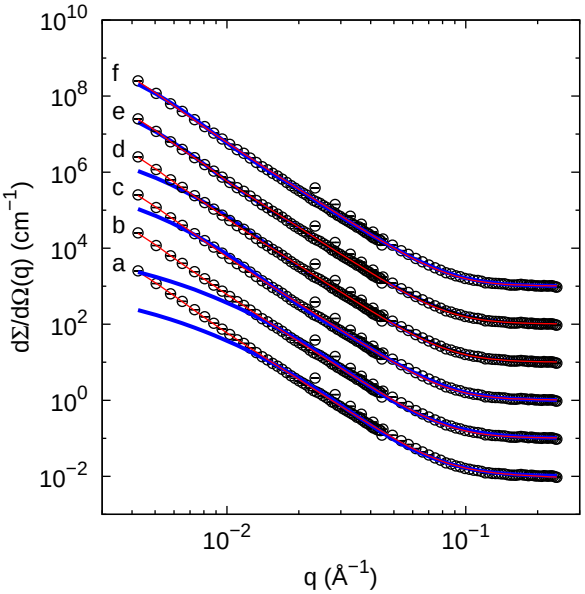

Figure 12: Fitting curves of the experimental SANS curve for the reference sample obtained by using $p = 2$, group I. Curves are scaled by a factor 10 for clarity. See the caption of Table 5 for the meaning of cases a-f. Red and blue curves refer to the analysis with GENFIT and MPS, respectively. Blue curves have been obtained with the same number N of cubic B-splines and the same average constrast used by GENFIT for cases a-f.

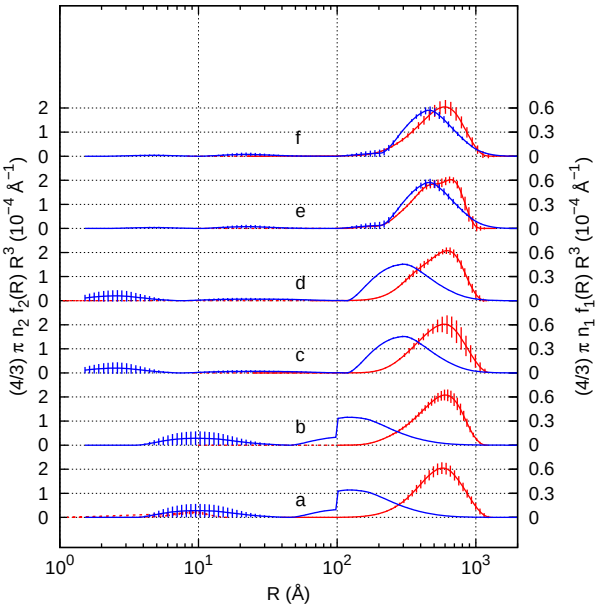

Figure 13: Volume distribution functions obtained by the analysis with $p = 2$ of the experimental SANS curve for the reference sample, group I. See the caption of Table 5 for the meaning of cases a-f. Red and blue curves refer to the analysis with GENFIT and MPS, respectively. Red solid and dotted lines, represented in the right and in the left y-axis, refer to the distributions of precipitates ($j = 1$) and voids ($j = 2$) obtained with GENFIT, respectively. Blue curves, obtained with the same number N of cubic B-splines and the same average contrast used by GENFIT for cases a-f, are represented in the right and in the left y-axis for $R > 10^2$ Å and $R \leq 10^2$ Å, respectively.

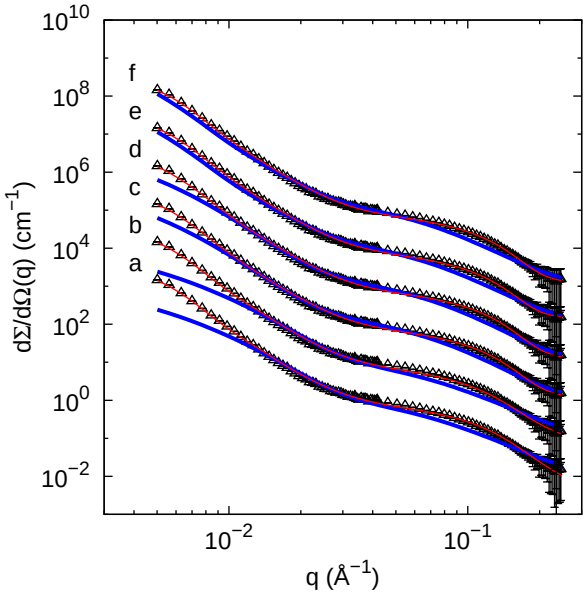

Figure 14: Fitting curves of the experimental SANS curve for the irradiated sample obtained by using $p = 2$, group I. See the caption of Fig. 12 for details.

		a	b	c	d	e	f
χ^2		1.73	1.87	1.43	1.81	1.50	1.36
U		0	0.75	0	0.09	0	0.07
$\mathcal{H}$		1.73	2.63	1.43	1.89	1.50	1.43
B		0.002±0.003	0.006±0.002	0.009±0.001	0.0079±0.0009	0.010±0.001	0.008±0.001
ϕ_1		0.0272±0.0007	0.0271±0.0005	0.0273±0.0003	0.0277±0.0005	0.0273±0.0003	0.0270±0.0005
$R_{1,\mathrm{mix}}$	(Å)	59±6	59±7	20±2	5±9	16±8	22±7
$R_{1,\mathrm{max}}$	(Å)	840±30	840±10	860±20	910±40	850±20	820±10
$c_{1,1}$		0.00±0.08	0.20±0.06	0.3±0.1	0.23±0.04	0.0±0.1	0.18±0.06
$c_{1,2}$		0.4±0.1	0.22±0.04	0.2±0.1	0.19±0.04	0.18±0.09	0.12±0.06
$c_{1,3}$		0.36±0.07	0.34±0.04	0	0.22±0.08	0.2±0.1	0
$c_{1,4}$		0.28±0.07	0.24±0.04	0	0.16±0.08	0	0
$c_{1,5}$		0	0	0.31±0.06	0	0.0±0.1	0
$c_{1,6}$		0	0	0.20±0.05	0.21±0.05	0.2±0.1	0.27±0.09
$c_{1,7}$		0	0	0	0	0.28±0.08	0.28±0.06
$c_{1,8}$		0	0	0	0	0.13±0.05	0.15±0.05
ϕ_2		0.0041±0.0003	0.0037±0.0002	0.0034±0.0001	$(352\pm6)\cdot10^{-5}$	0.0033±0.0001	0.0035±0.0001
$R_{2,\mathrm{mix}}$	(Å)	2±1	2.8±0.6	2±1	4±2	1.0±0.6	4±1
$R_{2,\mathrm{max}}$	(Å)	59±7	59±6	35±2	33±2	34.8±0.8	39±4
$c_{2,1}$		0.4±0.1	0.40±0.05	0.1±0.1	0.11±0.06	0.15±0.06	0.12±0.03
$c_{2,2}$		0.32±0.08	0.37±0.05	0.3±0.1	0.13±0.04	0.09±0.04	0.14±0.03
$c_{2,3}$		0.2±0.1	0.23±0.08	0.0±0.1	0.20±0.05	0.19±0.03	0.18±0.05
$c_{2,4}$		0	0	0.0±0.2	0.20±0.05	0.07±0.05	0.12±0.03
$c_{2,5}$		0	0	0.25±0.09	0.20±0.05	0.18±0.04	0.14±0.02
$c_{2,6}$		0	0	0.3±0.1	0.16±0.03	0.16±0.06	0.16±0.03
$c_{2,7}$		0	0	0	0	0.01±0.06	0.13±0.05
$c_{2,8}$		0	0	0	0	0.14±0.03	0.01±0.01
ϕ_{MPS}		0.028	0.030	0.032	0.032	0.044	0.043

Table 6: Fitting parameters from the GENFIT analyses with $p = 2$ of the experimental SANS curve for the irradiated sample, group I. ϕ_{MPS} values refer to the MPS analyses. See the caption of Table 5 for the meaning of cases a-f.

the experiment is very high, as confirmed by the values of χ^2 close to 1 shown in Table 6. The volume fraction of the precipitates, calculated as an average over the six cases a-f, turns out to be 0.0273 ± 0.0002, slightly lower than the one of the not irradiated sample (0.0317 ± 0.0006). The more interesting difference with respect to the previous curve is the presence of voids that GENFIT always finds, independently on the number of splines and regularization: as shown in Table 6, the value of ϕ_2, although small, is found with low uncertainty and, calculated as an average over the six cases a-f, corresponds to 0.0036 ± 0.0003.

The stability of these results can be clearly ascertained by looking to the volume distribution functions, $\frac{4}{3}\pi n_1 f_1(R)R^3$ and $\frac{4}{3}\pi n_2 f_2(R)R^3$, reported as solid and dotted red lines in Fig. 15. Notice that, in order to emphasize the difference of the two distributions, we have chosen two different y-scales. There are not appreciable differences among the cases: the most stable and less modulated result is obtained for the case b, with only $N = 4$ cubic B-splines and the regularization.

Poor results, for this curve, have been obtained by us by using the MPS software: all the fitting curves, shown as solid blue lines in Fig. 14, are quite far from the experimental points, also for the cases e and f ($N = 8$), which are, however, the best ones. Looking to the volume distribution function in Fig. 15 for the cases e and f, we can see that only the positions of the blue peaks are close to the ones of the red distributions, but not the height. As a consequence, the volume fractions calculated via MPS and reported in the bottom of Table 6 (0.044 and 0.043, cases e and f) are rather different from the values of ϕ_1 and ϕ_2 found by GENFIT.

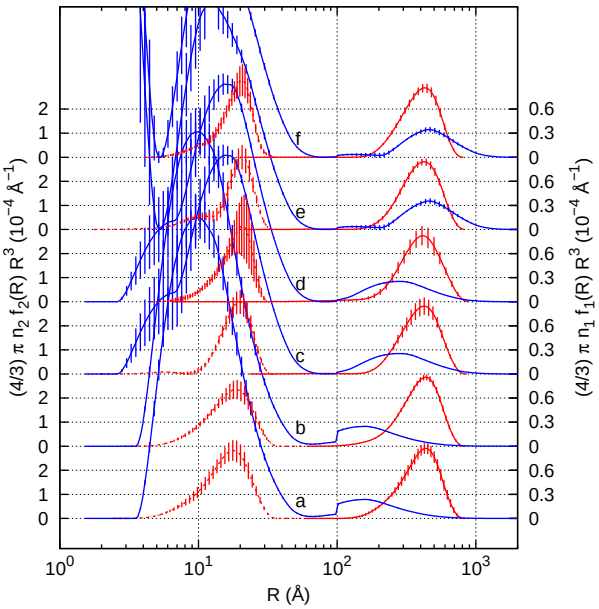

Figure 15: Volume distribution functions obtained by the analysis with $p = 2$ of the experimental SANS curve for the irradiated sample, group I. See the caption of Fig. 13 for details.

Group II: fitting of the experimental SANS curves with the hypothesis of one family of spherical inhomogeneities ($p = 1$) of unknown origin

In the second group of analyses, the GENFIT method has been applied by using the assumption that only one kind of inhomogeneity ($p = 1$) is present in the samples, with a unique effective scattering length density ρ_1, which is optimized between the two values which corresponds to carbide precipitates and voids ($\rho_1 = 5.30 \cdot 10^{-6}$ Å^{-2} and $\rho = 0$, respectively), and by using the value of ρ_0 corresponding to the metal alloy, as before ($7.55 \cdot 10^{-6}$ Å^{-2}). For this group, the comparison with MPS method is more straightforward, since it also assumes one kind for inhomogeneity, with polydispersed spherical shape. All resulting parameters are reported in Tables 7-8. Fitting curves and distributions functions are shown in Figs. 16-18 and in Figs. 17-20, respectively.

Concerning the refrence, not-irradiated sample, the GENFIT fitting curves, reported as red solid curves in Fig. 16, do not vary with respect to the ones obtained in the previous group of analysis: the χ^2s are all close to 1 (Table 7). In particular, the best analysis, both in terms of χ^2 and stability of the volume distribution function (see Fig. 17), is the one of case f ($N = 8$ and regularization). Notice that our MPS analysis with 8 splines is the unique that reaches an acceptable fit to the data (blue curves cases e and f in Fig. 16).

As a consequence, the inhomogeneity volume fractions obtained by GENFIT and MPS are very close only in this case (Table 7, case f) and correspond to 0.029 ± 0.001 and 0.026, respectively. We also notice that the scattering length density ρ_1 of the precipitates fitted by GENFIT (and used as input parameter for MPS) is $(5.21 \pm 0.04) \cdot 10^{-6}$ Å^{-2}, very close to the value $5.30 \cdot 10^{-6}$ Å^{-2} used in both simulations (see the caption of Fig. 2) and analyses of the experimental curves, group I.

The last fit concerns the analysis of the irradiated sample, which in the previous analysis has been described as constituted by both precipitates ($\phi_1 = 0.0273 \pm 0.0002$) and voids ($\phi_2 =$

		a	b	c	d	e	f
χ^2		1.10	1.10	1.21	1.07	1.20	1.06
U		0	0.02	0	0.01	0	0.02
$\mathcal{H}$		1.10	1.15	1.21	1.07	1.20	1.06
B		0.0101±0.0003	0.0101±0.0004	0.0101±0.0005	0.0101±0.0004	0.0101±0.0003	0.0101±0.0003
ρ_1	(10^{-6} Å^{-2})	4.4±0.5	5.0±0.3	4±1	3.7±0.4	5.1±0.7	5.21±0.04
ϕ_1		0.017±0.006	0.025±0.006	0.012±0.009	0.011±0.002	0.027±0.007	0.029±0.001
$R_{1,\mathrm{mix}}$	(Å)	130±30	120±10	50±60	150±10	4±1	170±10
$R_{1,\mathrm{max}}$	(Å)	1800±300	1900±300	1900±300	1100±200	1300±100	1090±90
$c_{1,1}$		0.5±0.1	0.52±0.05	0.22±0.08	0.29±0.04	0.16±0.05	0.23±0.09
$c_{1,2}$		0.3±0.1	0.32±0.05	0.14±0.08	0.24±0.04	0.16±0.06	0.19±0.09
$c_{1,3}$		0.15±0.06	0.16±0.03	0.3±0.1	0.21±0.05	0.11±0.05	0.2±0.1
$c_{1,4}$		0	0	0.25±0.08	0.14±0.03	0.15±0.06	0.16±0.07
$c_{1,5}$		0	0	0.12±0.09	0.08±0.02	0.16±0.07	0.10±0.07
$c_{1,6}$		0	0	0.00±0.07	0.04±0.02	0	0.08±0.06
$c_{1,7}$		0	0	0	0	0.17±0.04	0.04±0.02
$c_{1,8}$		0	0	0	0	0.10±0.04	0.03±0.03
ϕ_{MPS}		0.005	0.007	0.007	0.006	0.024	0.026

Table 7: Fitting parameters from the GENFIT analyses with $p = 1$ of the experimental SANS curve for the not-irradiated, reference sample, group II. ϕ_{MPS}s refer to the MPS analyses.

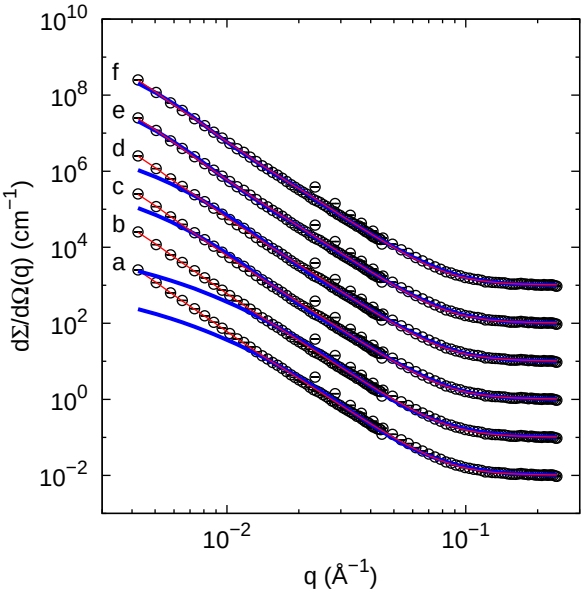

Figure 16: Fitting curves of the experimental SANS curve for the reference, not-irradiated sample obtained by using $p = 1$, group II. See the caption of Fig. 12 for details.

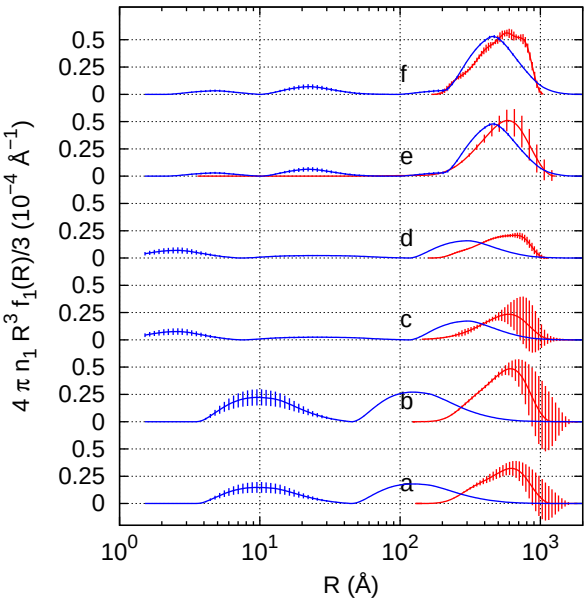

Figure 17: Volume distribution functions obtained by the analysis with $p = 1$ of the experimental SANS curves for the not-irradiated, reference sample, group II. See the caption of Table 5 for the meaning of cases a-f. Red and blue curves refer to the analysis with GENFIT and MPS, respectively. Blue curves, obtained with the same number N of cubic B-splines and the same average constrast used by GENFIT for cases a-f, are represented in the right and in the left y-axis for $R > 10^2$ Å and $R \leq 10^2$ Å, respectively.

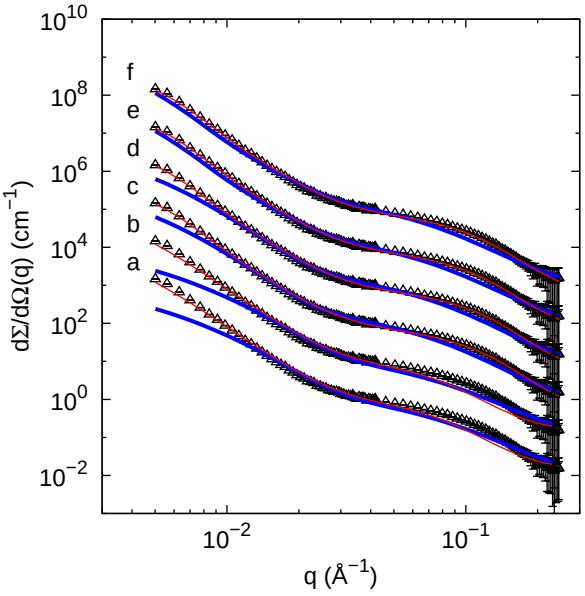

Figure 18: Fitting curves of the experimental SANS curve for the irradiated sample obtained by using $p = 1$, group II. See the caption of Fig. 12 for details.

0.0036±0.0003). The GENFIT results based on the assumption of only one type of inhomogeneity are quite poor, as well as the ones already obtained by us with MPS for the same SANS curve (see Fig. 18). However, the best solution if found for the case f, i.e. with the maximum number of cubic B-splines (see Table 8). Although for this case the χ^2 is quite good (1.88, see Table 8), a deepest observation of the residual plots compared to the ones obtained of by the GENFIT analyses of the same curve in the group I (see Fig. 19) clearly shows that the assumption of only one kind of inhomogeneity is overall worse than the one with two inhomogeneities.

The comparison of the unique volume distribution function between GENFIT and MPS methods is reported in Fig. 20 (red and blue curves, respectivley). The case f ($N = 8$ and regularization) is the one with the better overlap as, on the other hand, confirmed by the similarity between the volume fractions calculated with the two methods and shown in Table 8, which read 0.028 ± 0.002 and 0.028, respectively.

Results from the fitting analysis of the experimental SANS curves

According to the simulation tests, it appears very clear that a good fit of SANS curves can be obtained only under proper and appropriate hypotheses. Moreover, fitting results obtained by us using the MPS method appear to depend on the number of used B-splines even in the reference sample, suggesting that fitting results should be carefully considered. On the other side, the subroutine here derived, implemented inside the GENFIT software package, gives very stable solutions, especially when "regularization" methods are applied. In particular, even when the analysis is performed under the hypothesis that all the inhomogeneities in the matrix are to be described by only one average contrast, a few structural information concerning at least inhomogeneity size and size distribution can be derived. However, it should be clear that such a result is only qualitative: for example, the obtained volume fractions are widely underestimated or overestimated. Indeed, it is very easy to apply the GENFIT software package considering at

		a	b	c	d	e	f
χ^2		9.28	9.27	1.86	1.76	1.87	1.88
U		0	0.50	0	0.50	0	0.05
$\mathcal{H}$		9.28	9.77	1.86	2.26	1.87	1.91
B		0.0144±0.0008	0.0146±0.0006	0.005±0.001	0.005±0.001	0.006±0.001	0.0043±0.0009
ρ_1	(10^{-6} Å^{-2})	3.3±0.2	4.2±0.3	3.5±0.2	2.8±0.4	4.9±0.2	4.0±0.2
ϕ_1		0.014±0.001	0.023±0.004	0.022±0.002	0.016±0.003	0.049±0.008	0.028±0.002
$R_{1,\mathrm{mix}}$	(Å)	1.000±0.007	$(1000000\pm2)\cdot10^{-6}$	3.1±0.1	3.11±0.07	1.00±0.01	1.00±0.01
$R_{1,\mathrm{max}}$	(Å)	1080±10	1096±9	948±8	951±9	922±8	920±10
$c_{1,1}$		$(99999\pm2)\cdot10^{-5}$	$(9999930\pm9)\cdot10^{-7}$	0.999±0.002	$(100000\pm2)\cdot10^{-5}$	0.4±0.1	0.46±0.06
$c_{1,2}$		0	0	0	0	0.27±0.07	0.34±0.06
$c_{1,3}$		0	0	0	0	0.30±0.08	0.19±0.05
$c_{1,4}$		0	0	0	0	0	0
$c_{1,5}$		0	0	0	0	0	0
$c_{1,6}$		0	0	0	0	0	0
$c_{1,7}$		0	0	0	0	0	0
$c_{1,8}$		0	0	0	0	0	0
ϕ_{MPS}		0.014	0.022	0.016	0.012	0.050	0.028

Table 8: Fitting parameters from the GENFIT analyses with $p = 1$ of the experimental SANS curve for the irradiated sample, group II. See the caption of Table 5 for the meaning of cases a-f. ϕ_{MPS}s refer to the MPS analyses.

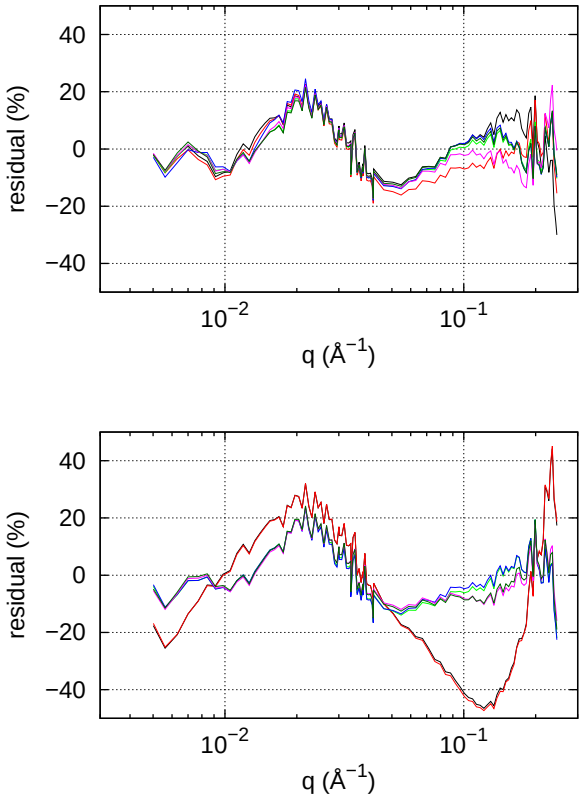

Figure 19: Residual plots, $[\frac{d\Sigma}{d\Omega}(q) - \frac{d\Sigma}{d\Omega}_{\mathrm{exp}}(q)]/\frac{d\Sigma}{d\Omega}_{\mathrm{exp}}(q)$, of the GENFIT analyes shown in Fig. 14 (upper frame) and in Fig. 18 (lower frame). Black curves, case a. Red curves, case b. Green curves, case c. Blue curves, case d. Magenta curves, case e. Dark-green curves, case f.

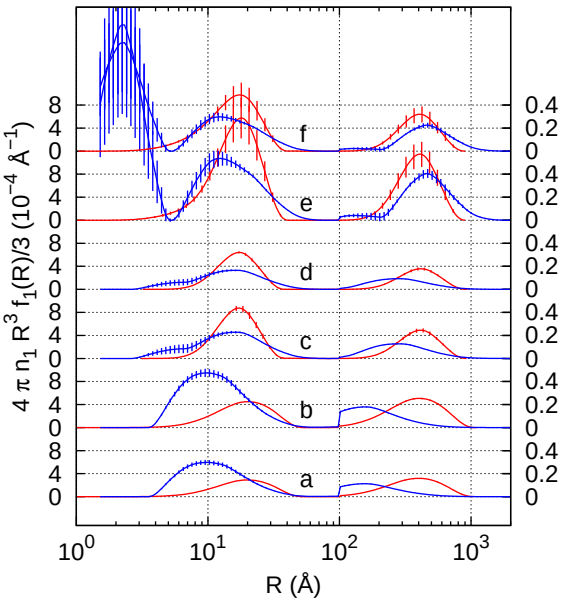

Figure 20: Volume distribution functions obtained by the analysis with $p = 1$ of the experimental SANS curve for the irradiated sample, group II. See the caption of Fig. 17 for details.

least two particle families of different contrast, size and size distribution (this option is not implemented in the MPS program). In such a condition, the fitting curves reproduce with very high accuracy the experimental data in all the measured q-range and the fitted parameters appear robust and trustable.

Final comments

In the present study, we extended the use of the cubic B-spline approach for a quantitative analysis of SANS curves obtained from metal alloys containing up to a maximum of two different kind of inhomogeneities (namely, precipitates and voids), each one characterized by a specific scattering length density. After formalization of this new approach, and the implementation of the method inside the GENFIT software package, a test case has been considered: the SANS signal of a sample of Eurofer alloy before and after being subjected to irradiation in a nuclear reactor has been analyzed by us, comparing MPS and the new GENFIT software packages. Results have been discussed in terms of the number of cubic B-splines used and of the selection of "regularization" constraints. As a result, it appears very clear that a good fit of SANS curves can be obtained only under proper and appropriate hypotheses, but while fitting results obtained by us using the MPS method appear to strongly depend on the considered q-range and on the number of used B-splines even in the reference sample (where only carbide precipitates are expected), the new GENFIT subroutine gives very stable solutions, especially when "regularization" methods are applied, reproducing with very high accuracy the experimental data in all the measured q-range and conditions.

Bibliography

1. Magnani, M., P. Puliti, and M. Stefanon, 1988. Numerical solution of the inverse problem in the analysis of neutron small angle scattering experiments. *Nucl. Instr. and Meth. A* 271:611–616.

2. Coppola, R., R. Kampmann, M. Magnani, and P. Staron, 1998. Microstructural investigation, using polarized neutron scattering, of a martensitic steel for fusion reactors. *Acta Mater.* 46:5447–5456.

3. Coppola, R., R. Lindau, R. P. May, A. Möslang, and M. Valli, 2009. Investigation of microstructural evolution under neutron irradiation in Eurofer97 steel by means of small-angle neutron scattering. *J. Nuc. Mater.* 386-388:195–198.

4. Coppola, R., M. Klimenkov, R. Lindau, A. Möslang, M. Valli, and A. Wiedenmann, 2011. Recent applications of small-angle neutron scattering in the characterization of irradiated steels for nuclear technologies. *J. Nuc. Mater.* 409:100–105.

5. Prautzsch, H., W. Boehm, and M. Paluzny, 2002. Bèzier and B-Spline Techniques. Springer Verlag.

6. Hansen, S., and J. S. Pedersen, 1991. A Comparison of Three Different Methods for Analysing Small-Angle Scattering Data. *J. Appl. Cryst.* 24:541–548.

7. Glatter, O., 2002. Fourier Transformation and Deconvolution. *In* P. Lindner, and T. Zemb, editors, Neutron, X-rays and Light. Scattering Methods Applied to Soft Condensed Matter, North-Holland, 103–124.

8. Spinozzi, F., 2008. *http://alisf1.univpm.it/biophysics/software.htm* .

9. Ortore, M. G., P. Mariani, F. Carsughi, S. Cinelli, G. Onori, J. Teixeira, and F. Spinozzi, 2011. Preferential solvation of lysozyme in water/ethanol mixtures. *J. Chem. Phys.* 135:245103–245111.

10. Ortore, M. G., F. Spinozzi, S. Vilasi, I. Sirangelo, G. Irace, A. Shukla, T. Narayanan, R. Sinibaldi, and P. Mariani, 2011. Time-resolved small-angle x-ray scattering study of the early stage of amyloid formation of an apomyoglobin mutant. *Phys. Rev. E.* 84:061904–061910.

11. Barbosa, L. R. S., M. G. Ortore, F. Spinozzi, P. Mariani, S. Bernstorff, and R. Itri, 2010. The Importance of Protein-Protein Interactions on the pH-Induced Conformational Changes of Bovine Serum Albumin: A Small-Angle X-Ray Scattering Study. *Biophys. J.* 98:147–157.

12. Kirkpatrick, S., C. D. Gelatt, and M. P. Vecchi, 1983. Optimization by Simulated Annealing. *Science* 220:671–680.

13. 2000. 2000 Index, Computing in Science and Engineering, Volume 2. *Computing in Science and Engineering* 2:94–97.

14. Spinozzi, F., D. Gazzillo, A. Giacometti, P. Mariani, and F. Carsughi, 2002. Interaction of proteins in solution from small angle scattering: a perturbative approach. *Biophys. J.* 82:2165–2175.

FULLPROF analysis of neutron diffraction data on Eurofer-97 martensitic steel containing Y_2O_3 nanoparticles

Introduction

The investigated material is oxide-dispersion strengthened (ODS) Eurofer-97 martensitic steel (8.9 Cr, 1.1 W, 0.2 V, 0.14 Ta, 0.42 Mn, 0,11 C wt%), that is being developed for future fusion reactors. In this material, in particular, Y_2O_3 nanoparticles were dispersed into the steel matrix with a nominal content of 0.5 wt%. Such a system was previously studied by SANS [R. Coppola et al., Physica B 350 (2004) e545-e548], and, as a result, the size distributions of Y_2O_3 nanoparticles were obtained, in a very good agreement with TEM observations.

The aim of the neutron diffraction experiment was the detection (despite the low content of the particles) of the Y_2O_3 diffraction peaks and possibly the determination of their crystallographic features inside the Eurofer-97 matrix.

Material and Experimental data

The investigated material is oxide-dispersion strengthened (ODS) Eurofer-97 martensitic steel (8.9 Cr, 1.1 W, 0.2 V, 0.14 Ta, 0.42 Mn, 0.11 C wt%). In the present investigated material, Y_2O_3 nanoparticles are dispersed into the steel matrix, with a nominal content of 0.5 wt%. Diffraction experiments were performed at the D1A neutron diffractometer of ILL - Grenoble, using a wavelength of 0.191 nm.

Rietveld refinement

The diffraction patterns were analyzed using the Rietveld refinement technique: the neutron or X-ray diffraction of powder samples results in a pattern characterised by reflections (peaks in intensity) at certain positions, the height, width and position of which can be used to determine many aspects of the materials structure.

In particular, a powder diffraction pattern can be recorded in numerical form for a discrete set of scattering angles, times of flight or energies (the scattering variable generally indicated as T). Then, the experimental powder diffraction pattern is usually given as two arrays $\{T_i, y_i\}$. In the case of data that have been manipulated or normalized in some way, the three arrays $\{T_i, y_i, \sigma_i\}$, where σ_i is the standard deviation of the profile intensity y_i, are needed in order to properly weight the residuals in the least squares procedure. The profile can be modeled using the calculated counts $y_{c,i}$ at the i-th step by summing the contribution from neighbouring Bragg reflections plus the background:

$$y_{c,i} = \sum_{\phi} S_{\phi} \sum_{\mathbf{h}} I_{\phi,\mathbf{h}} \Omega(T_i - T_{\phi,\mathbf{h}}) + b_i \tag{1}$$

The vector $\mathbf{h}$ labels the Bragg reflections, the subscript ϕ labels the phase.

The general expression of the integrated intensity is:

$$I_{\phi,\mathbf{h}} = \{LAPCF^2\}_{\phi,\mathbf{h}} \tag{2}$$

The meaning of the different terms appearing in Eqs. 1 and 2 is the following:

- S_ϕ is the scale factor of the phase ϕ
- $L_{\mathbf{h}}$ contains the Lorentz, polarisation and multiplicity factors
- $F_{\mathbf{h}}$ is the structure factor
- $A_{\mathbf{h}}$ is the absorption correction
- $P_{\mathbf{h}}$ is the preferred orientation function
- Ω is the reflection profile function that models both instrumental and sample effects
- $C_{\mathbf{h}}$ includes special corrections (non linearity, efficiencies, special absorption corrections, extinction, etc.)
- b_i is the background intensity

Different functions can be chosen to represent the peak shape: Gaussian, Lorentzian, Pearson-7, Pseudo-Voigt.

The Rietveld Method consists of refining a crystal structure by minimizing the weighted squared difference between the observed y_i and the calculated pattern $y_{c,i}$, against the parameter vector $\boldsymbol{\alpha} = \{\alpha_1, \alpha_2, \ldots, \alpha_p\}$. The function minimised in the Rietveld Method is

$$\chi^2 = \sum_{i=1}^{n} w_i \{y_i - y_{c,i}(\boldsymbol{\alpha})\}^2 \tag{3}$$

with $w_i = 1/\sigma_i^2$, σ_i being the variance of y_i.

Running the fullprof program

The FULLPROF program has been mainly developed for Rietveld analysis [H.M. Rietveld, Acta Cryst. **22**, 151 (1967); H.M. Rietveld, J. Applied Cryst. **2**, 65 (1969); A.W. Hewat, Harwell Report No. 73/239, ILL Report No. 74/H62S; G. Malmros & J.O. Thomas, J. Applied Cryst. **10**, 7 (1977); C.P. Khattak & D.E. Cox, J. Applied Cryst. **10**, 405 (1977)] (structure profile refinement) of neutron (nuclear and magnetic scattering) or X-ray powder diffraction data collected at constant or variable step in scattering angle 2θ. The program can be also used as a Profile Matching (or pattern decomposition) tool, without the knowledge of the structure. Single Crystal refinements can also be performed alone or in combination with powder data. Time-of-flight (TOF) neutron data analysis is also available. Energy dispersive X-ray data can also be treated but only for profile matching.

Input files

filename.pcr

Input control file, containing crystallographic data. This file is normally updated, or written to **filename.new**, every time the program is run.

filename.dat

Intensity data file, its format depends on the instrument. This corresponds to the profile intensity of a powder diffraction pattern.

filename.bac

Background file. The program uses this file to calculate the background at each value of the scattering variable. The program may generate this file, from refined polynomial or interpolated data, if the user asks for it. In the presented case, the background has been refined using a linear interpolation between the 14 given points.

myresol.irf

File describing the instrumental resolution function. In the presented case, the instrumental resolution was contained in the D1A_19A280606.irf file and was obtained using $Na_2Ca_3Al_2F_{14}$.

Output files

filename.out

This is the main output file that contains all control variables and refined parameters.

filename.prf

Observed and calculated profile, to be fed into visualisation programs.

filename.sum

Parameter list after last cycle: summary of the last parameters, their standard deviations and reliability factors.

filenameN.mic

File containing microstructural information for the N-th phase.

Refinement results

In the present case, the refinement was carried out assuming the possible presence of four different phases:

1. α-Fe: body-centered cubic space lattice (space group: Im3m), cell parameter: 0.287 nm, density 7.847 g/cm^3.
2. Y_2O_3: body-centered cubic space lattice (space group: Ia-3), cell parameter 1.06 nm, density 5.031 g/cm^3.
3. Fe_3O_4 (*magnetite*): face-centered cubic space lattice (space group: Fd-3m), cell parameter 0.84 nm, density 5.176 g/cm^3.

4. $M_{23}C_6$ (*carbides precipitates*): body-centered cubic space lattice (space group: Fm3m), cell parameter 1.066 nm, density 0.306 g/cm^3.

The background was refined using a linear interpolation on 14 given points.

While the experimental diffraction pattern and the corresponding refinement curve are shown in Fig. 1, the fitting results are reported in the .out and .sum output files which have

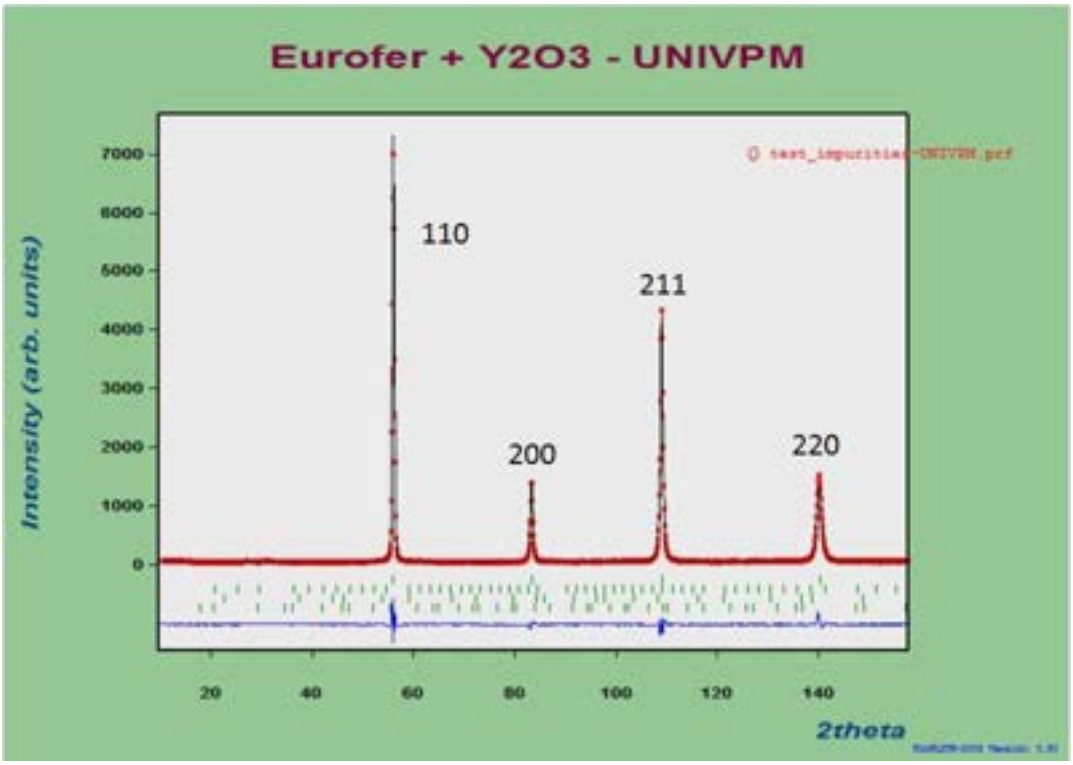

Figure 1: Diffraction pattern and corresponding refinement curve; only peaks corresponding to α-Fe are visible at this scale.

been included in the Appendix B. The same Appendix also reports the output microstructure (.mic) files for phases 1, 2 and 4 described above, since the phase 3 turned out to be absent in the investigated material.

In Fig. 1 only the peaks corresponding to α-Fe are visible, due to the fact that the content of this phase is actually exceeding 99% wt. Anyway, by looking at the output files, the FULLPROF refinement gives some information for the other phases too. In particular, Fig. 2 shows the observed and calculated (from Rietveld refinement) diffraction patterns for Y_2O_3. According to the good superposition of the observed and calculated peak spacings and the rather excellent reproducibility of the relative peak intensities, the presence of Y_2O_3 body-centered cubic Ia-3 phase is strongly suggested.

The following Table reports the percentage of the integrated diffraction intensity from each phase (the Rietveld results are reported in Appendix B, .sum file, for sake of completeness):

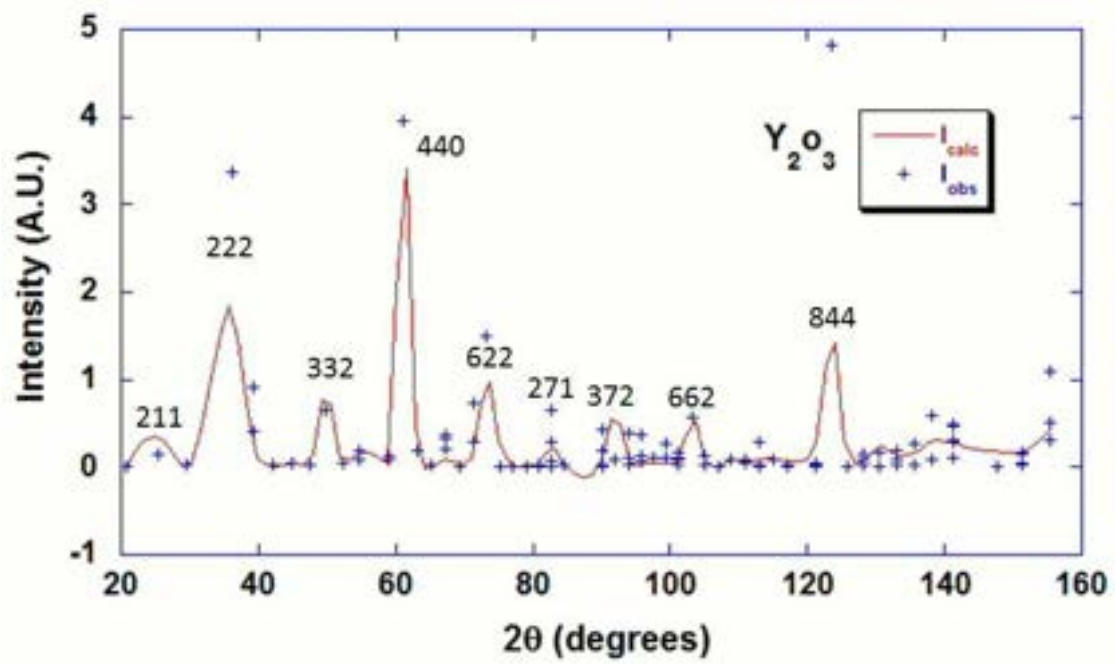

Figure 2: Calculated and observed (from Rietveld refinement) diffraction patterns for Y_2O_3 nanoparticles.

Phase	*%Cont*	*Nintdp*	*Nprofp*	*Nref*
1	99.54	1	6	4
2	0.32	0	1	118
3	0.00	0	1	26
4	0.14	0	1	56

where *%Cont* is the percentage of diffracted intensity of each phase with respect to the total integrated intensity (100×), *Nintdp* is the number of intensity-affecting refined parameters, *Nprofp* is the number of profile refined parameters and *Nref* is the number of contributing reflections. Results are interesting as the indication that Y_2O_3 diffraction peaks only provide the 0.3 % of the integrated intensity is in full agreement with the very low content of Y_2O_3 nanoparticles inside the Eurofer-97 (the nominal content is 0.5 wt%). According to the very low diffracted intensity, however, an accurate analysis of the background will be necessary to confirm the presence of the Y_2O_3 phase.

Conclusion

The presented Rietveld analysis of the considered diffraction pattern is actually able to demonstrate the presence of Y_2O_3 phase (body-centered cubic space lattice, space group: Ia-3) inside the Eurofer-97 matrix, with a content compatible to the expected one. However, an accurate analysis of the background will be necessary to confirm such a result.